



## Assessing diversity, abundance, and mass of microplastics (~ 1–300 $\mu\text{m}$ ) in aquatic systems

Luis E. Medina Faull , Tatiana Zaliznyak, Gordon T. Taylor \*

School of Marine and Atmospheric Sciences, Stony Brook University, Stony Brook, New York

### Abstract

Recent improvements in survey methods for microplastic (MP) pollution in natural waters have enabled quantification of MP particles < 300  $\mu\text{m}$  in diameter. Historically, this putatively important size fraction of MP particles has not been sampled adequately, possibly leading to significant underestimations of plastic inventories in aquatic systems. Furthermore, reported MP particle numbers are poorly constrained proxies for MP mass loadings as sizes vary widely and densities differ within and among polymers, consequently compromising mass flux estimations. However, determination of MP number, identity, and mass can resolve these issues and enable more accurate estimations of MP loadings. Using Raman microspectroscopy coupled with three-dimensional (3D) spectral imaging, we have developed an automatable methodology to detect, identify, and quantify MPs retained on filters from discrete water samples. Raman spectral information enabled identification of plastic polymers in particles between 0.5 and 300  $\mu\text{m}$  in diameter and generation of 3D chemical maps. To accelerate volume determinations of each identified MP particle, we developed an algorithm to derive volumes from image analysis of two-dimensional micrographs that are statistically indistinguishable from those directly measured by 3D Raman chemical maps. Masses of each Raman-identified MP particle are determined from their volumes and known plastic specific weights. This methodology provides accurate estimations of the smallest MP particles' contributions to total MP mass in discrete water samples, providing vital information for mass flux calculations of MPs in natural waters.

Microplastics (MPs) have become an omnipresent component of the man-made litter that pollutes aquatic environments. These micro-sized particles, whose diameters range from 5 mm down to submicron, are intentionally produced (e.g., microbeads in personal care and cleaning products, industrial pellets, etc.) or are derived from breakdown of larger plastic items and synthetic fabrics (Arthur et al. 2009). Most MP debris in marine ecosystems originates from inland sources and is transported to coastal areas by rivers (Martin et al. 2017; Zhang 2017), discharged by municipal water pollution control plants (WPCPs) (Alimi et al. 2018), or discharged as urban surface runoff (Mintening et al. 2017). Once entering coastal areas, MPs can be transported vertically, laterally along the coast or moved to the open ocean by currents, tides, and winds (Rios et al. 2010; Enders et al. 2015; Kanhai et al. 2017).

As a consequence of aggregation and vertical transport, significant amounts of MPs reach the seabed or lake beds and accumulate in benthic habitats, where they are ingested by diverse groups of organisms, including commercially important mollusk

and fish species (Imhof et al. 2012; Woodall et al. 2014; Martin et al. 2017). However, the actual consequences of MPs in aquatic food webs are still largely unknown (Lohmann 2017). For instance, MPs are known to adsorb persistent organic contaminants, such as polychlorinated biphenyls and polyaromatic hydrocarbons, from the water column or sediment pore waters. Hence, MPs have been hypothesized to serve as efficient carriers of harmful organic contaminants into food webs, enhancing bioaccumulation in upper trophic levels (Zettler et al. 2013). Furthermore, MPs originating from WPCPs or discharged as urban runoff could act as transport vectors for attached/sorbed pathogenic microorganisms. For example, Oberbeckmann et al. (2018) reported that potential pathogenic Enterobacteriaceae were abundant on polypropylene (PP) particles in a Baltic Sea estuary near a municipal WPCP.

Current estimates based on models developed mainly using surface net tow data indicate that approximately 5.25 trillion plastic particles, ranging in size from macro- to micro-sized (> 300  $\mu\text{m}$ ) and weighing about 269,000 metric tons, have found their way into surface waters of the global ocean (Eriksen et al. 2014). However, this mass only accounts for about 1% of the mismanaged plastic waste stream reportedly entering the oceans annually (Jambeck et al. 2015).

\*Correspondence: gordon.taylor@stonybrook.edu

Additional Supporting Information may be found in the online version of this article.

One likely factor contributing to this mismatch is that techniques used to sample, detect, and identify MPs almost exclusively account for particles captured in plankton nets (i.e.,  $> 330 \mu\text{m}$ ) and ignore a potentially important fraction of smaller plastic debris (Conkle et al. 2018; Covernton et al. 2019; Lindeque et al. 2020). While commonly employed net tows for MP collection have advantages, such as enabling collection from large water volumes (Conkle et al. 2018), they primarily sample buoyant materials in surface waters. However, they are incapable of resolving vertical distributions of MPs associated with nonbuoyant material (Hidalgo-Ruz et al. 2012; Covernton et al. 2019; Lindeque et al. 2020). Moreover, most existing MP studies have focused on enumerating generic MP particles, and not on their identity or mass, precluding accurate estimations of plastic mass fluxes in natural waters (Shim et al. 2017).

Fortunately, recent improvements in sampling and analytical practices have facilitated better characterization of smaller MP size fractions ( $< 330 \mu\text{m}$ ). For example, Enders et al. (2015) collected large quantities of MP particles ( $> 10 \mu\text{m}$ ) from the North Atlantic Ocean using a vessel-mounted underway filtration system. Additionally, analytical methods, such as vibrational microspectroscopies (Raman and Fourier-transform infrared [FTIR]), have enabled accurate identification of MP polymers using characteristic spectral features (Käppler et al. 2015). MP polymers in particles as small as  $10 \mu\text{m}$  have been now identified by FTIR and  $5 \mu\text{m}$  by Raman microspectroscopy (Primpke et al. 2017; Araujo et al. 2018).

Recently, Primpke et al. (2020) and Zarfl (2019) summarized amenable approaches for Raman microspectroscopic analysis of MPs. For example, facile identification of chemical structure and quantification of MP particles  $< 20 \mu\text{m}$  in natural samples has been accomplished by point-by-point mapping (Käppler et al. 2016) and an automated “Particle Finding” algorithm (Frère et al. 2016; Brandt et al. 2020). In addition, stimulated Raman scattering has been demonstrated to reduce analysis time of environmental samples but is limited to detection of MP  $> 12 \mu\text{m}$  (Zada et al. 2018). The technique described in this communication can detect and identify MP particles as small as  $0.46 \mu\text{m}$ . The described approach facilitates detection of many of the smallest MP particles suspended in natural waters and allows for estimation of MP concentration, particle size, and mass.

We applied Raman microspectroscopy to survey all MP particles larger than our filter pore size ( $0.2 \mu\text{m}$ ) in discrete seawater samples (several milliliters to liters), which enables vertical sampling of the entire water column. While applied to seawater samples, we see no impediments to applying these methods to freshwater systems. Our goal was to devise an automatable technique to detect, identify, and quantify submicrometer- to submillimeter-sized MPs directly captured on filters. In addition, by coupling Raman microspectroscopy with spectral imaging, we generated three-dimensional (3D) chemical maps of particles based on intensities of diagnostic spectral peaks for a

given polymer. From these maps, particle volumes were calculated and compared to volumes and masses determined by independent methods. We demonstrate that knowledge of the identity and volume of an individual MP particle enables accurate determination of the particle’s mass. We contend that mass-based estimations of MP inventories will provide more meaningful assessments of MP fluxes in aquatic systems than those derived from particle numbers.

## Materials and procedures

Protocols developed in this study are primarily based on Raman microspectroscopy and follow a workflow (Fig. 1) designed to minimize human intervention and reduce sampling processing steps.

### Preparation of standard MP suspensions

The first step was to validate Raman microspectroscopic detection of MP particles of different sizes, shapes, and polymer compositions when captured on filters. For this, MP particles ranging from  $\sim 1 \mu\text{m}$  to a few millimeters in diameter and composed of different plastic polymers (e.g., polypropylene [PP], polyethylene [PE], polystyrene [PS], polycarbonate [PC], polyethylene terephthalate, different types of rubbers, several types of inks commonly used in the laboratory, xanthan glue, polyvinyl chloride [PVC], polyvinyl sulfide) were generated as

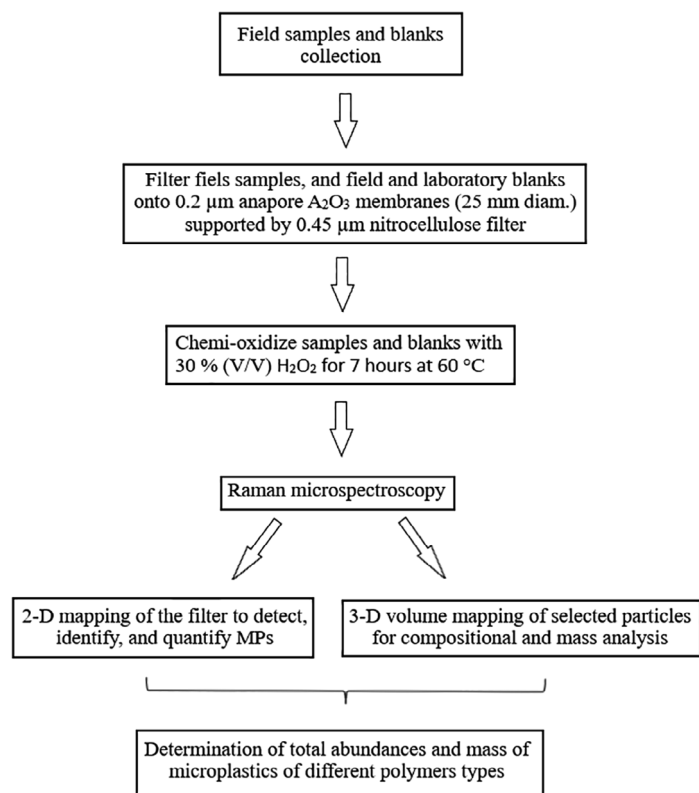


**Fig. 1.** Schematic outline of the Raman-based workflow for quantifying MPs in aquatic samples.

mixed standard suspensions from random macro-plastic particles ( $> 5$  mm) that were manually collected from an anthropogenically impacted sandy beach (Port Jefferson, New York). These particles were representative of the complex chemical character of environmental plastics resulting from exposure to natural weathering, as well as being potentially colonized and degraded by microorganisms. These processes likely alter the chemical composition of MPs compared to the virgin plastics often used in other studies. After collection, macroparticles were fragmented using a commercial blender (Waring). The ground plastic suspension was sequentially segregated into particle size classes of  $> 650$ ,  $650\text{--}200$ ,  $200\text{--}120$ ,  $120\text{--}60$ , and  $< 60$   $\mu\text{m}$  using analytical stainless-steel sieves (DIN 4188, Retsch GmbH, Germany). Each size class and a mixture of different size classes were suspended in filtered seawater ( $< 0.2$   $\mu\text{m}$ ) into individual glass containers to generate several standard MP suspensions (hereafter referred as MP standard suspensions) that were used to develop the protocol. To evaluate homogeneity of particle distributions on filters and to compare our measurement with two other independent methods, a diluted suspension of a known concentration of fluorescent microbeads (Fluoresbrite® polystyrene microspheres,  $0.46$   $\mu\text{m}$  diameter, Polysciences) was prepared (hereafter referred as fluorescent microbeads). All MP standard suspension, fluorescent microbeads, and natural water samples were filtered onto  $\text{Al}_2\text{O}_3$  membrane filters bonded to an annular polypropylene ring (Anodisc™, 25 mm diameter,  $0.2$   $\mu\text{m}$  pore size, Whatman®) and analyzed using Raman microspectroscopy (described below).

### Collection and preparation of natural water samples for MP quantification

Surface-water samples from three stations off the southern coast of Long Island (New York Bight, New York, U.S.A.) were collected using standard rosette-mounted PVC Niskin bottles and transferred directly into 0.5-liter glass bottles. This non-selective approach captures all particles within a volume, including the micron-sized particles ( $< 300$   $\mu\text{m}$ ) that are excluded from many published MP surveys sampled by plankton net tows. Care was taken to rinse the Niskin bottles' interior and the glass bottles with filtered Milli-Q water before sampling to minimize MP contamination. To account for possible sampling contamination, a field blank was prepared by filling a rinsed Niskin bottle with particle-free Milli-Q™ water and sampling it the same way as for the environmental samples.

Once in the lab, water from each glass bottle was passed through a  $200$   $\mu\text{m}$  metal sieve (DIN 4188, Retsch GmbH) to separate MPs into two size categories. However, we note that no particles  $> 200$   $\mu\text{m}$  were found in any of field samples presented herein. The  $< 200$   $\mu\text{m}$  fractions were stored in glass bottles and later filtered onto  $\text{Al}_2\text{O}_3$  membrane filters (Anodisc™, 25 mm diameter,  $0.2$   $\mu\text{m}$  pore size, Whatman®). To minimize analytical interference from abundant biogenic particles,

samples were cleaned by chemi-oxidation (described below) prior to Raman microspectroscopic analysis. Laboratory blanks were prepared by passing  $0.5$  L of prefiltered MilliQ™ water through an  $\text{Al}_2\text{O}_3$  membrane filters and subjecting them to the same procedures as samples.

### Filtration of MP standard suspensions and natural water samples

Previous experience applying Raman microspectroscopy demonstrated that Anodisc™  $\text{Al}_2\text{O}_3$  filters are the best choice for this application because they are “Raman-silent” in the spectral regions diagnostic for plastics, unlike nitrocellulose, glass fiber, or polycarbonate filters. Furthermore, these filters are available in a pore size ( $0.2$   $\mu\text{m}$ ) small enough to retain most particles of interest. In addition, these filters offer a relatively flat surface minimizing variations in focal planes across and among microscopic fields. MP standard suspensions, environmental samples, and blanks were filtered within a laminar flow hood onto these Anodisc™ filters using an all glass filtration apparatus, including a sintered glass filter support in the base with a metal clamp. Due to the filter's inherent brittleness, care was taken not to bend Anodisc™ filters during mounting and removal by exclusively handling the filter by the annular polypropylene ring bonded to the membrane. While processing samples, personnel wore cotton laboratory coats in order to minimize plastic contamination from synthetic fabrics and did not wear gloves. Before and between filtration steps, the filtration apparatus was washed with filtered ( $0.22$   $\mu\text{m}$ ), distilled water and covered with clean aluminum foil. Personnel manipulating samples washed hands before the filtration process and between samples.

In early trials, using the MP standard suspensions and fluorescent microbeads, the filtration process led to heterogeneous distributions of particles on the filters. As reported by Loder et al. (2015), uneven MP particle distributions on filter surfaces can lead to a significant bias if total particle concentrations are extrapolated from subsampling a filter. To reduce particle distribution heterogeneity, we evaluated effects of introducing a backing filter to distribute vacuum pressure more uniformly. Replicate suspensions of diluted fluorescent microbeads were captured on either the  $0.2$   $\mu\text{m}$  Anodisc™ filter alone or on the Anodisc™ supported on a nitrocellulose filter saturated with MilliQ™ water (25 mm diameter,  $0.45$   $\mu\text{m}$  pore size; Millipore™). Results (see “Assessment” section) indicated that Anodiscs™ mounted on supporting nitrocellulose filters yielded relatively homogeneous distributions of MP particles across the entire filter, significantly reducing possible biases in counts. This method was used for all quantitative analyses.

### Chemi-oxidation of natural water samples

In environmental samples (water, sediments, and organisms), the presence of organic matter on the filters presents a challenge for Raman microspectroscopic analysis. To

avoid possible interference between signals from often fluorescent biogenic and synthetic (MP) organic matter, a chemi-oxidation step was performed during filtration. While the filtered sample was still in the filtration apparatus, ~ 10 mL of hydrogen peroxide (30% V/V) was added. Then the entire apparatus (filter support, clamp, and funnel) securely covered with aluminum foil was moved to an oven and allowed to sit for 7 h at 60°C (modified from Tagg et al. 2015). An average 3–4 samples were filtered and purified per work session. After the digestion procedure, filters were rinsed with Milli-Q water, mounted on a glass slides without a cover slip, and analyzed directly under the Raman microspectrophotometer.

### Validation of Raman microspectroscopic quantification of MP particles

Epifluorescence microscopy and flow cytometry were used to validate MP particle counts determined by Raman microspectroscopy. For this, dilute suspensions of 0.46  $\mu\text{m}$  fluorescent microbeads were filtered onto a 0.2  $\mu\text{m}$  Anodisc™ mounted on a supporting nitrocellulose filter and analyzed using Raman microspectroscopy. Microbeads on the same Anodisc™ filter were enumerated on a Zeiss AxioScope epifluorescent microscope. A replicate suspension was analyzed directly on a Beckman Coulter CytoFLEX flow cytometer. Total particle counts obtained by epifluorescence microscopy and flow cytometry were used to assess the accuracy and analytical uncertainty of counts obtained by our Raman microspectroscopic method.

### Raman microspectroscopic analysis of filtered MP particles

A Renishaw® inVia™ confocal Raman microspectrophotometer was used to identify and quantify MP particles captured on filters. The microspectrophotometer is configured with a modified upright Leica® DM2700™ epifluorescence microscope, a computer-controlled motorized x-y-z stage with 0.1  $\mu\text{m}$  step size in all dimensions, four laser lines (457/514 nm Ar + ion laser, 633 nm He/Ne laser, 785 nm diode laser), and a 1040  $\times$  256 Peltier-cooled CCD detector.

Standard suspensions of field-collected MPs were used initially to determine the optimal instrument configuration (choices of laser line and power, diffraction grating, detector exposure time, objective lens) for efficient mapping. For most analyses, a grid was set up within a region of interest (ROI) and spot spectra were taken every 1  $\mu\text{m}$  in x and y dimensions, which combined with the objective lens and laser wavelength define the theoretical spatial resolution ( $r$ ) and spatial coverage of the method. For example, focusing the 633 nm laser through our N Plan Epi 50x/0.75 NA objective lens (#566072, Leica, Germany) yields a theoretical resolution ( $r = 0.61\lambda/\text{NA}$ ) of objects greater than 0.51  $\mu\text{m}$  apart. The confocal laser beam spot diameter at the sample is approximately twice  $r$  or 1.03  $\mu\text{m}$ . Thus, if an ROI on the filter is sampled at 1  $\times$  1  $\mu\text{m}$  step sizes in x- and y-dimensions, then essentially 100% of the total ROI area has been interrogated.

More than 300 ROIs from different filters capturing MPs from the standard suspensions were scanned using the Stream Line® image acquisition feature in the software WiRE™ 5.2 (Renishaw®). The highest quality spectra and optimal sample throughput were obtained applying the 633 nm He/Ne laser at ~ 9.3 mW power at the sample through the  $\times 50$  objective lens. Spectra were acquired using a 1200 lines  $\text{mm}^{-1}$  diffraction grating, a spectral range of 200–2500  $\text{cm}^{-1}$ , and single detector exposures of 0.7 s spectrum $^{-1}$ . These instrumental settings were applied for all reported analyses.

For environmental samples, each filter was scanned over 33 ROIs that were randomly selected to represent MP distributions across the entire exposed filter area. Each ROI was defined as a 100  $\times$  100  $\mu\text{m}^2$  grid in the camera image, equivalent to a 10,000  $\mu\text{m}^2$  area, and interrogated through the  $\times 50$  objective lens. Using 1  $\times$  1  $\mu\text{m}$  step sizes on the automated stage resulted in collection of 10,000 spectra from a single ROI. The total time to acquire data from each ROI was 90 min resulting in a total of 49.5 h to complete 33 ROI.

After automated data collection, the Stream Line® feature (Renishaw® WiRE™ 5.2) was used to revisit spatial coordinates of plastic-like particles in each ROI and produce detailed two-dimensional (2D) chemical maps. Chemical maps were created from all spectra using component analysis (non-negative least squares correlation method, according to Renishaw® application note # AN224(EN)-01-A, 2019). This analysis simplified data evaluation and decreased data processing time considerably. To verify particle identities, Raman spectra from each particle were compared to a reference library of >300 known plastic polymers (KnowItAll Raman Spectral Library, BIO-RAD®, U.S.A.). Library matches with a score greater than 60 (internal library score 0–100) were accepted as positive identifications for that material (Woodall et al. 2014). In addition to using the reference library (KnowItAll Spectral Library, BIO-RAD®) in the NAno-Raman Image Laboratory (NARMIL), we developed an internal library for synthetic and natural materials with high quality authentic standards. We used this library as a complementary method to assure that each particle found on the filters was correctly assigned to a specific material.

### Filter-based quantitative enumeration of MP particles

After totaling the number of particles from the 33 ROIs, the number of MP particles per liter of sample ( $N$ ) was calculated in the same manner as for epifluorescence enumeration of microorganisms, according to Eq. 1.

$$N = \frac{Af * n}{b * M * V} \quad (1)$$

where  $Af$  is the total exposed filter area ( $\text{mm}^2$ ),  $n$  the total number of MP particles counted summed across all ROI,  $b$  the number of ROI examined,  $M$  the area size of one ROI ( $\text{mm}^2$ ), and  $V$  the volume (L) of the water filtered from the sample.

The analytical uncertainty of the total number of particle ( $N$ ) in each sample was established calculating the standard error from all 33 ROI counted per sample. Total number of particles per L are reported as  $N \pm 1SE$ .

### Particle size, volume, and mass calculations

With the aid of image analysis software (Renishaw® WiRE™ 5.2), the dimensions, area, and equivalent spherical diameter (ESD) of each particle were determined. The area was determined by counting total plastic-positive pixels assigned to each particle image. This particle area ( $A_p$ ) was used to calculate the ESD by applying eq. 2 from Engel (2009):

$$ESD = \left(\sqrt{A_p/\pi}\right) * 2 \quad (2)$$

With this information, an idealized volume estimate for each particle was calculated. The wide range of MP shapes likely impacts volume calculations. We sought a geometric model that approximated a large variety of shape possibilities and that could be applied broadly to particles while also minimizing required microscopic measurements. The ellipse is among the best because it exhibits flexibility in its ratio of minor and major axes and can approximate both spheroids and oblong fibers, for example. We concluded that MP particles are best represented by ellipsoids as described by Hillebrand et al.'s (1999) equation (Eq. 3).

$$V = \frac{4}{3} * \pi * (ESD/2)^3 \quad (3)$$

This volume estimate model based on 2D mapping is hereafter referred to as the "2D volume."

In order to establish how accurately the "2D volumes" estimated above approximate true particle volumes, actual 3D maps were produced by Raman microspectroscopy on select MP particles. An important and unique feature of this technique is that it can generate accurate 3D spatial images of micron-sized particles based on detection of diagnostic Raman spectral peak intensities. However, one drawback to this approach is that it can be time-consuming, especially for larger particles mapped at high spatial resolution. For this reason, we limited our analysis to 31 particles ranging from 1 to 200  $\mu\text{m}$  ESD, more or less covering the size range targeted by our methodology. A 3D chemical map was generated for each particle using the volume image acquisition routine provided in the instrument's software (Renishaw® WiRE™ 5.2). Spectra were produced using the 633 nm He/Ne laser at  $\sim 9.3$  mW laser power at the sample through the  $\times 50$  objective lens with detector exposure times of 1 s spectrum<sup>-1</sup>. The motorized stage was programmed to move the sample under the laser at step sizes ranging from 0.2 to 10  $\mu\text{m}$  in x-, y-, and z-dimensions, depending on the particle size. Raman-based volume estimates were calculated by summing all plastic-positive pixels from 3D maps of each particle. The total time to acquire data from each

particle varied from 15 min to 5 h, depending on the particle's size. These volumes are hereafter referred to as 3D volumes.

With the goal of producing accurate volume measurements to derive mass estimates of all MP particles surveyed, the time-consuming 3D volume measurements were compared to the rapid "2D volume" estimates for the same 31 particles. The relationship of the two independent measurements of particle volume was evaluated by least squares linear regression analysis and Kuskal-Wallis test of significance. Masses of each plastic polymer in the MP pool were then calculated using both 2D and 3D volume estimates and published specific weights (density =  $\text{g cm}^{-3}$ ) of the plastic polymers identified from each particle. We note that density of a specific polymer can vary depending on formulation and weathering (Supporting Information Table S4). Thus, we applied mean literature values and observed variance in our calculations. In order to estimate the uncertainty propagated in the mass calculation (Mass R.E.) for each particle, analytical uncertainty in both the volume algorithm and the mean density were considered the following equation was applied (Harris 2010):

$$\text{Mass R.E.} = \sqrt{(\text{R.E.vol})^2 + (\text{R.E.den})^2} \quad (4)$$

where R.E. vol is the relative error (SE of the slope/slope) of the linear regression slope (3D and "2D volume"). R.E. den is the relative variations (SE/mean) in the range of reported density values (Supporting Information Table S4) for each polymer contained in a specific particle. To account for total propagated uncertainties when extrapolating from mass to total microplastic load per liter (Total MP load in  $\mu\text{g L}^{-1} \pm 1SE$ . See Table 1), we added a relative error term for MP particle concentration to Eq. 4.

## Assessment

### Analysis of MP particles in standard suspensions

In order to demonstrate that our methodology can recognize and accurately enumerate small MP particles on Anodisc™ filters, results from enumerating fluorescent microbeads in replicate subsamples by Raman microspectroscopy, epifluorescence microscopy, and flow cytometry were compared. Calculated microbead abundances from Raman microspectroscopy ( $1.9 \pm 0.10 \times 10^{10}$  particles L<sup>-1</sup>) were not significantly different ( $p > 0.05$ ; Kruskal-Wallis test of significance) from three replicates measured by epifluorescence microscopy ( $1.7 \pm 0.14 \times 10^{10}$  particles L<sup>-1</sup>), or by flow cytometry ( $1.5 \pm 0.22 \times 10^{10}$  particles L<sup>-1</sup>) (note: unless otherwise specified,  $N \pm$  value represents the mean  $\pm 1SD$  hereafter). Analytical uncertainty (error) for the Raman-based census was low and comparable to flow cytometric measurements and was lower than for epifluorescence microscopy, that is, relative standard deviations (RSDs) were 4.6%, 4.4%, and 7.4%, respectively. It is also noteworthy that by using the Raman microspectrophotometer setup described above, we were able to detect single MP particles as small as 0.46  $\mu\text{m}$  in diameter (Fig. 2).

The same suspension of fluorescent microbeads was also used to optimize particle distribution on 0.2  $\mu\text{m}$  Anodisc™ filters. Microbead distributions across the surface of an Anodisc™ filter placed directly on the sintered glass filtration base were patchy (Fig. 3a). Passing a duplicate subsample through an Anodisc™ filter mounted on a water-saturated nitrocellulose supporting filter reduced patchiness significantly (Fig. 3b). For each duplicate sample, we counted particles in 30 ROI, calculated the mean and the SD, and repeated twice to obtain the RSD among the triplicates. When using Anodisc™ filters placed directly on the sintered glass filtration base (no nitrocellulose supporting filter), the mean microbead counts and 1 SD for each ROI were 318 ( $\pm 112$ ), 296 ( $\pm 121$ ), and 277 ( $\pm 119$ ) with an average RSD of 40% among the triplicate subsamples. In contrast, Anodisc™ filters mounted on a water-saturated nitrocellulose supporting filter provided a significantly more homogeneous spatial distribution. The average number of particles in each ROI among the triplicate subsamples were similar, but analytical uncertainties were much improved: 266 ( $\pm 15$ ), 313 ( $\pm 24$ ), and 289 ( $\pm 21$ ) with an average RSD of 7% among the triplicate subsamples. These results demonstrate that utilizing the supporting filter produces a relatively homogeneous particle distribution and enables extrapolation of MP counts from randomly selected ROI to total number of MP particles on a filter.

The MP standard suspensions of beach-collected, sieved MPs were used to demonstrate that MP particles of different sizes, shape, color, additive composition, state of degradation, and polymer composition are accurately recognized using our methodology. More than 300 ROI from filters capturing MPs from the standard suspensions were analyzed by Raman microspectroscopy. Two examples that demonstrate the ability of this method to identify types of polymers and their pigments and additives from a wide range of particle sizes are presented in Fig. 4. Detected particles from the standard suspensions varied in diameter from 1 to  $\sim 1000 \mu\text{m}$ . In the first example, six  $\sim 1 \mu\text{m}$  diameter particles, all appearing similar in morphology by reflected bright-field microscopy, were

interrogated by Raman and color-coded based on their composition (Fig. 4a). Intense Raman peaks at 1000, 1580, and 1600  $\text{cm}^{-1}$  indicated that four of these particles (yellow) were composed of primarily of PS. These same spectra also exhibited two other diagnostic peaks indicative of titanium dioxide (515 and 635  $\text{cm}^{-1}$ ), a well-known additive used by plastic manufacturers. Within the same microscopic field, the Raman-scattered peak at 460  $\text{cm}^{-1}$  indicated that the remaining three  $1 \mu\text{m}$  particles (green) were composed of quartz. In the second example (Fig. 4b), Raman mapping revealed two adjacent and visually indistinguishable particles that were chemically distinct. Raman-scattered peaks at 808, 840, and 1460  $\text{cm}^{-1}$  revealed that the larger particle (102  $\mu\text{m}$  diameter) was primarily PP (red), while peaks at 678, 744, and 1520  $\text{cm}^{-1}$  established that the smaller 35  $\mu\text{m}$  particle was phthalocyanine copper blue (CuPc, blue) (Fig. 4b).

### MP particle volumes and masses

To validate MP volume estimates derived from 2D measurements, we compared them to 3D volume measurements of micron-scale particles produced by mapping intensities of diagnostic Raman spectral peaks in three dimensions. An advantage of Raman 3D spectral mapping is that it captures the complex shape of MP particles and makes no assumptions about the particle's geometry. As an example, an amorphous Raman-identified PP particle from the standard MP suspensions was mapped in 3D with  $1 \times 1 \times 1 \mu\text{m}$  (x-y-z) resolution based on the presence of the diagnostic 811 and 844  $\text{cm}^{-1}$  peaks (Fig. 5). The total number of  $1 \mu\text{m}^3$  cubes with positively identified PP peaks was summed, resulting in a particle volume of 7547  $\mu\text{m}^3$ . Using a PP density ( $\pm$  SE) of  $0.89 \pm 0.008 \text{ g cm}^{-3}$  yields a total mass ( $\pm$  SE) of  $6.6 \pm 0.18 \text{ ng}$  for this particle. For comparison, image analysis applied to the reflected bright-field micrograph of the same particle yields a 2D area of 452  $\mu\text{m}^2$ . Applying our “2D volume” algorithm to this area yields an ESD of 24  $\mu\text{m}$  and the best-fit ellipse enclosing the particle has a volume ( $\pm$  SE) of

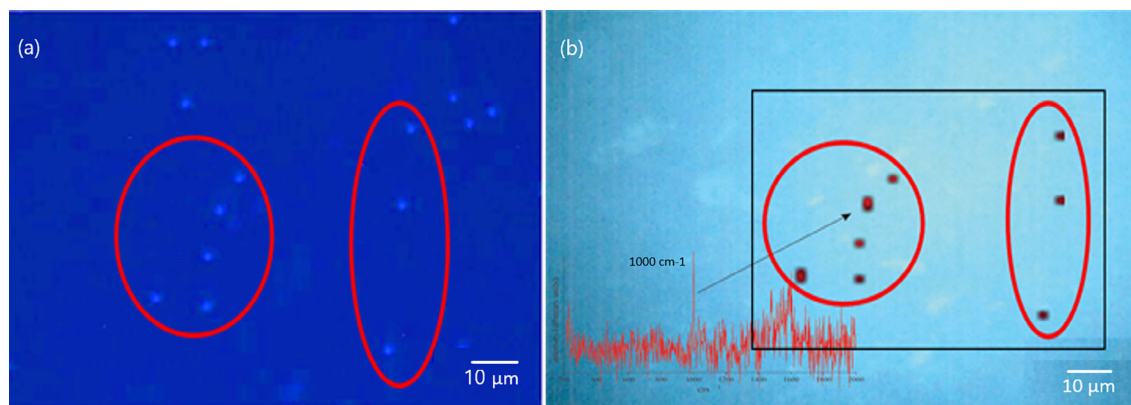


**Fig. 2.** (a) Epifluorescent micrographs of 0.46  $\mu\text{m}$  Fluoresbrite® polystyrene microbeads captured on an Anodisc™ filter. (b) Composite image of Raman chemical maps of the same polystyrene microbeads in (a) superimposed on reflected light micrographs of the sampled filters.

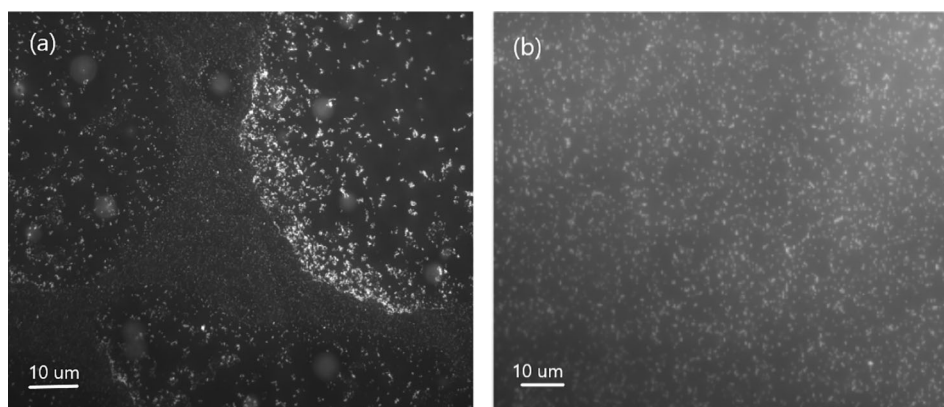


**Fig. 3.** (a) Monochromatic epifluorescent micrograph of  $0.46\ \mu\text{m}$  Fluoresbrite® polystyrene microbeads captured on an Anodisc™ filter without the nitrocellulose supporting filter. (b) Micrograph of same microbeads captured on Anodisc™ filters with supporting nitrocellulose filter. Micrographs acquired under  $\times 1000$  magnification.

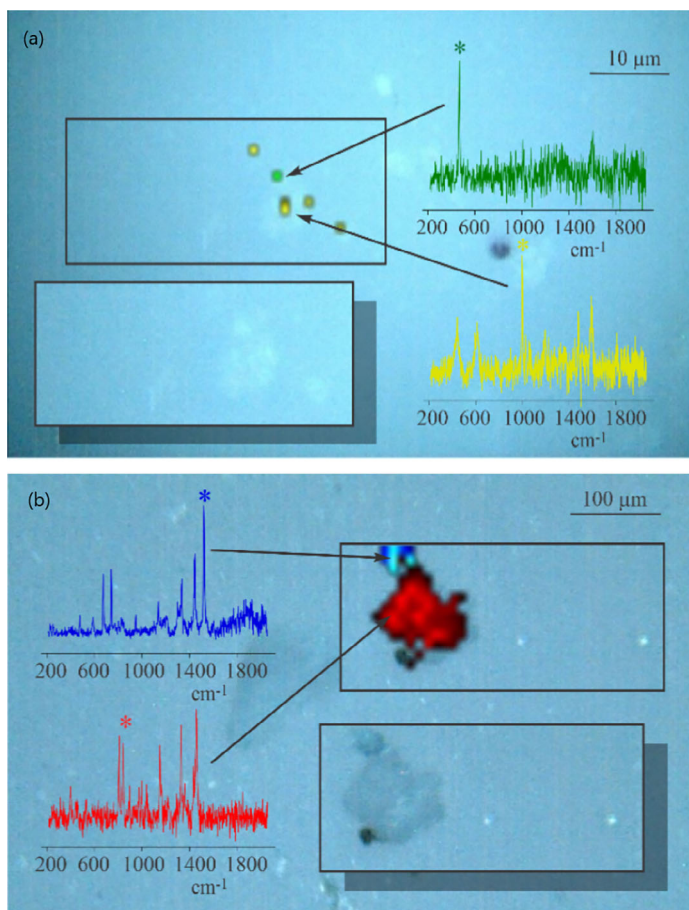


**Fig. 4.** Composite images of Raman chemical maps superimposed on micrographs of the sampled filters. Floating rectangles in (a) and (b) are reflected bright-field micrographs of the mapped regions of interest (ROI). Chemical maps in upper rectangles are color-coded based on diagnostic Raman peaks (\*) produced by individual particles, examples of which are superimposed on micrographs. (a) Four polystyrene MP particles

$7229\ \mu\text{m}^3 \pm 168$ . This hypothetical volume generates a mass ( $\pm$  SE) of  $6.1 \pm 0.24\ \text{ng}$  for this PP (density of  $0.89 \pm 0.008\ \text{g cm}^{-3}$ ) particle.

To evaluate the robustness of the relationship between 2D-estimated and actual 3D volume determinations, we repeated the comparison on a subset of particles ( $n = 31$ ). Particles from our MP standard suspensions were captured on filters and represented a range of sizes (1–200  $\mu\text{m}$  in diameter), shapes, polymer compositions, and weathering states. Volumes derived from image analysis measurements of area, ESD, and our “2D volume” algorithm were not significantly different from actual Raman-based 3D volume measurements ( $p > 0.05$ ; Kruskal-Wallis test of significance). In fact, 2D and 3D volume determinations were highly correlated ( $r^2 = 0.98$ ) among the individual particles, with a regression slope approximating 1 ( $m \pm \text{SE} = 1.01 \pm 0.01$ ), and a y-intercept of  $76\ \mu\text{m}^3 (\pm 665\ \text{SE})$  indicating the two methods can be used interchangeably over the broad size range of MPs examined (Fig. 6a). The seemingly large y-intercept is indistinguishable from zero due to analytical uncertainty and may result from a slight slope break between small and larger particles. To confirm the strength of the relationship for the smallest particles, we examined the regression parameters for particles smaller than  $40 \times 10^3\ \mu\text{m}^3$  ( $n = 24$ ) (Fig. 6b). “2D volumes” were not significantly different from Raman-based 3D volume measurements ( $p > 0.05$ ; Kruskal-Wallis) for the smallest particles either. The regression remained strong ( $r^2 = 0.99$ ) with a slope still close to 1 ( $0.97 \pm 0.01$ ) and a smaller y-intercept of  $20\ \mu\text{m}^3 (\pm 96\ \text{SE})$ . Thus, even for particles  $< 40 \times 10^3\ \mu\text{m}^3$  ( $\sim 40\ \mu\text{m}$  ESD), the 2D estimation algorithm performs well for volume determinations.

The time required to acquire data for MP volume and mass surveys should be the deciding factor on the appropriate approach. Clearly, producing 3D Raman maps are more time-consuming and should be used only in specific situations

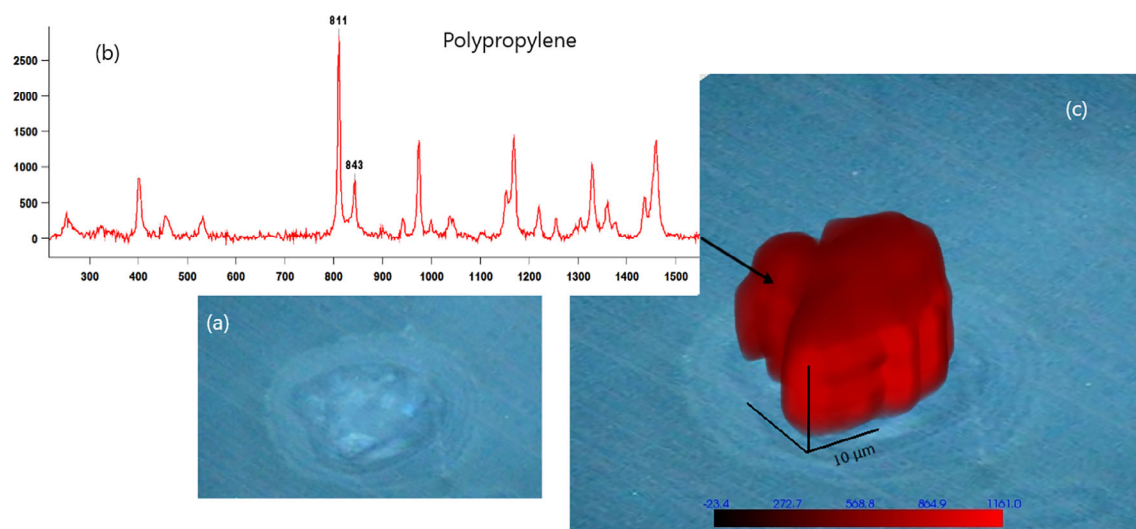


**Fig. 5.** Example of a 3D chemical map of a PP particle produced by our Raman microspectroscopic volume mapping routine. **(a)** Reflected bright-field micrograph of a MP particle. **(b)** Representative Raman spectrum from the particle revealing diagnostic peaks (808 and 840  $\text{cm}^{-1}$ ) for PP. **(c)** 3D chemical volume map of the particle based on distribution of a diagnostic PP Raman spectral peak (808  $\text{cm}^{-1}$ ).

where analysis of a single MP particle could resolve complex chemical structure that may be informative. For example, the total time to acquire all 7547 spectra required to produce the 3D map in Fig. 5c was approximately 90 min and the time required to batch process spectra and produce a single map was 2 h. Thus, for volume and mass surveys of environmental samples (reported below), a single Raman spectrum was first acquired to identify each individual MP particle and the “2D volume” estimation method was applied to captured reflected bright-field micrographs.

It is not uncommon in environmental samples for MP particles to have chemically complex structures. Knowledge about these complex compositions can be useful forensically to trace a contaminant back to its source. Several available tools can provide information on relative abundances of different plastic polymers in bulk samples, but very few can provide this information on individual MP particles. 3D Raman mapping is uniquely capable of resolving composite structures in individual MP particles at micron to submicron spatial scales. Figure 7 illustrates an example of a 3D chemical map of an environmental MP particle generated using diagnostic peaks for PP (red), CuPc (cyan), and pure PE (purple) and PE blended with CuPc (dark blue). This amorphous particle has a measured upper surface area of  $0.74 \text{ mm}^2$ , an ESD of  $0.97 \text{ mm}$ , and a volume of  $0.48 \text{ mm}^3$ . Based on this 3D chemical map, the volume of each polymer could be measured and the corresponding mass calculated. The particle is composed primarily of PE which was evident in pure form or in combination with the pigment CuPc, which accounted for about  $0.47 \text{ mm}^3$  or 97% of the particle volume and representing  $0.43 \text{ mg}$  of PE. However, a very strong and distinct PP Raman signal found in the center penetrating through most of the particle’s z-dimension and accounted for a volume of

$\sim 0.064 \text{ mm}^3$  (3% of the particle volume) and  $0.06 \text{ mg}$  of PP. Blended PP and PE is rare in manufactured products because these two polymers are immiscible with one another (Eagan et al. 2017). However, during the recycling process, they can be mixed and form recycled mixed polyolefin products (Hubo et al. 2016). This results in recycled blended items forming heterogeneous materials composed of unmixed islands of these two resins (Eagan et al. 2017). Consequently, single particle analysis can be used forensically to infer that particles, such as the one in Fig. 7, originate from secondary material sources that are produced from recycled mixed polymer waste (Hubo et al. 2016; Eagan et al. 2017).

### MP particles in environmental samples

We applied our method to a set of surface-water samples collected at  $\sim 1 \text{ m}$  depth from three stations off the southern coast of Long Island (New York Bight, New York, U.S.A.). Chosen stations were a subset of an 11-station study on water quality near the Southwest Sewer district outfall discharge (Fig. 8). Samples from these stations are expected to have a strong anthropogenic influence. Reported results are intended as proof-of-concept for our method, rather than a systematic study on water quality in the region. For each station,  $0.5 \text{ L}$  of water was filtered and the total number of particles found in 33 ROI from individual filters from all three stations ( $1.5 \text{ L}$  of water) was 96. The sample from Sta. 1 ( $40.58^\circ\text{N}$ ,  $73.45^\circ\text{W}$  nearshore – 1.18 nautical miles offshore) yielded 36 particles. Sta. 2 ( $40.57^\circ\text{N}$ ,  $73.45^\circ\text{W}$  approximately 1.99 nautical miles offshore) yielded 32 particles. And Sta. 3 ( $40.55^\circ\text{N}$ ,  $73.44^\circ\text{W}$  3.2 nautical miles offshore) provided 28 particles. PP particles were the most abundant MP in samples from all three stations, followed by PS, CuPc, and polytetrafluoroethylene (PTFE = Teflon). Two PC particles were found in the filter blank processed in the open laboratory and



**Table 1.** Characteristics of MP particles from three coastal stations.

Station	ROI counted/ filter	Total MP particles in all ROI (# part)	Mean particle ESD ( $\mu\text{m} \pm \text{SE}$ ) (min–max)	Total MP mass in all ROI <sup>a</sup> (ng $\pm$ SE)	Total MP concentration (# $\times 10^3 \text{ L}^{-1} \pm \text{SE}$ )	Total MP load <sup>b</sup> ( $\mu\text{g L}^{-1} \pm \text{SE}$ )
1	33	36	$1.7 \pm 0.10$ (1–2.8)	$0.15 \pm 0.001$	$96 \pm 12$	$0.38 \pm 0.08$
2	32	32	$2.5 \pm 0.34$ (1–9.5)	$1.94 \pm 0.01$	$83 \pm 11$	$5.03 \pm 0.70$
3	33	28	$2.9 \pm 0.48$ (1–12.3)	$1.78 \pm 0.02$	$73 \pm 0.9$	$4.49 \pm 0.60$
Field blank	33	0	0	0	X	X
Lab blank	33	2	$6.3$ (2.5–7.5)	0.12	X	X

<sup>a</sup>Total MP mass calculated directly from abundance, volumes, and specific weights of polymers found in all ROI.

<sup>b</sup>Total MP load estimated from each polymer's concentrations, volumes, and specific weights. Uncertainties in the extrapolated total microplastic load per liter (Total MP load =  $\text{ng L}^{-1} \pm \text{SE}$ ) were calculated by adding a relative error term for particle concentrations to Eq. 4 to account for total propagated error in the mass estimates.

no MP particles were observed in any other lab blank or in the field blank. Applying Eq. 1, we extrapolated the total number of particles across all ROI to MP particles per liter ( $N \pm 1 \text{ SE}$ ). MP concentrations in these surface-water samples varied from  $96 \pm 12 \times 10^3$  particles  $\text{L}^{-1}$  at Sta. 1 to  $83 \pm 11 \times 10^3$  particles  $\text{L}^{-1}$  at Sta. 2, and  $73 \pm 0.9 \times 10^3$  particles  $\text{L}^{-1}$  at Sta. 3.

Widely reported MP abundances are based primarily on samples collected by plankton net tows that exclude particles smaller than 330–500  $\mu\text{m}$ , depending on net mesh used. In our Niskin bottle-collected samples from these three coastal stations, the most numerically abundant MP particles captured on 0.2  $\mu\text{m}$  pore-size filters (25 mm diam.) were in the size range of 1–12.3  $\mu\text{m}$  ESD, with 96% of the particles being less than 5  $\mu\text{m}$  (Fig. 9). No particles larger than 13  $\mu\text{m}$  in diameter were detected in these samples.

Furthermore, the presieving step in sample processing failed to yield any particles larger than 200  $\mu\text{m}$  in any of these field samples, all underscoring the relative rarity of larger MP particles in 0.5 L of coastal seawater.

Particle size distributions varied slightly among the three stations. On average, MP particles were larger at Sta. 2 (ESD =  $2.5 \pm 2.0 \mu\text{m}$ ) and Sta. 3 (ESD =  $2.9 \pm 2.6 \mu\text{m}$ ), while the mean ESD at Sta. 1 was  $1.7 \pm 0.6 \mu\text{m}$ . However, this slight variation could have a great effect on particle mass measured at each station. Even though MP particle abundances were higher at Sta. 1, total MP mass ( $\pm \text{SE}$ ) estimated from each polymer's concentrations, volumes, and specific weights at Sta. 2 and 3 ( $5.03 \pm 0.70 \mu\text{g L}^{-1}$  and  $4.49 \pm 0.60 \mu\text{g L}^{-1}$ , respectively) were greater than at Sta. 1 ( $0.38 \pm 0.08 \mu\text{g L}^{-1}$ ), due to presence of slightly larger particles (Table 1). Interestingly, in

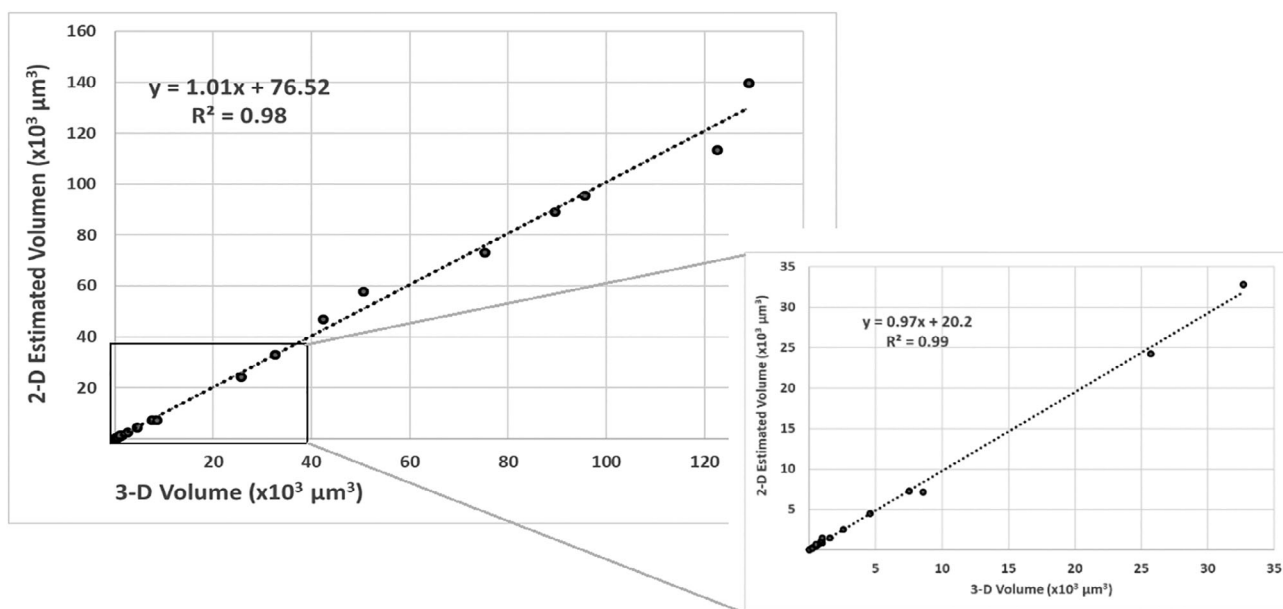


**Fig. 6.** Comparison of “2D volume” estimates based on image analysis and assumed ellipsoid geometry to Raman microspectroscopic 3D volume measurements. (a) For 31 individual MP particles ranging 1–200  $\mu\text{m}$  in diameter. (b) For 24 individual MP particles ranging 1–40  $\mu\text{m}$  in diameter.

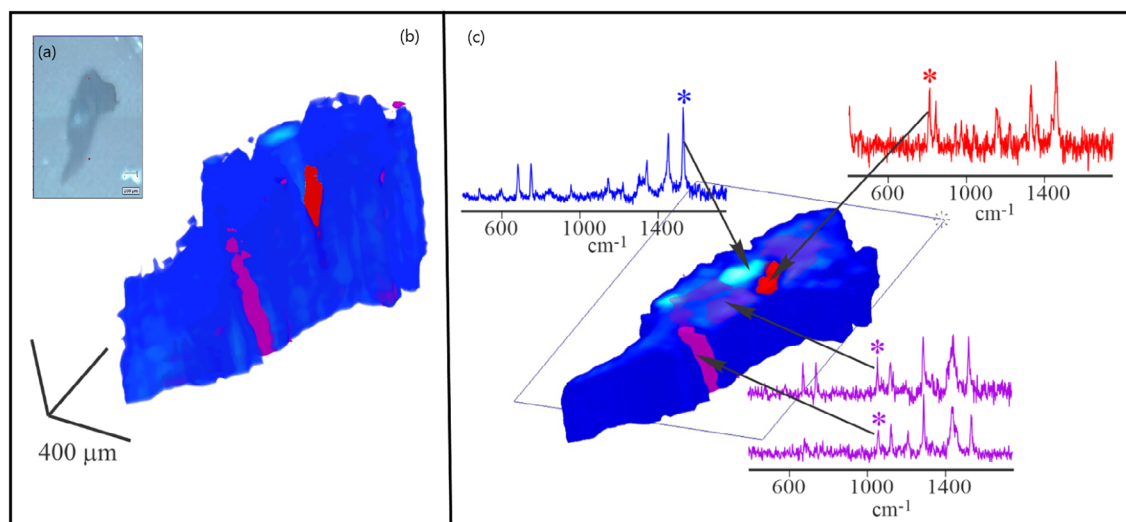


**Fig. 7.** 3D chemical maps of a composite MP particle produced by Raman microspectroscopic volume mapping. Particle captured on an  $\text{Al}_2\text{O}_3$  Anodisc™ filter was from the standard suspension of beach collected and sieved MPs. **(a)** Reflected bright-field micrograph of an MP particle captured on the filter. **(b)** 3D chemical map of the entire MP particle generated from diagnostic peaks of PP (red), phthalocyanine blue copper (cyan), and PE (purple).

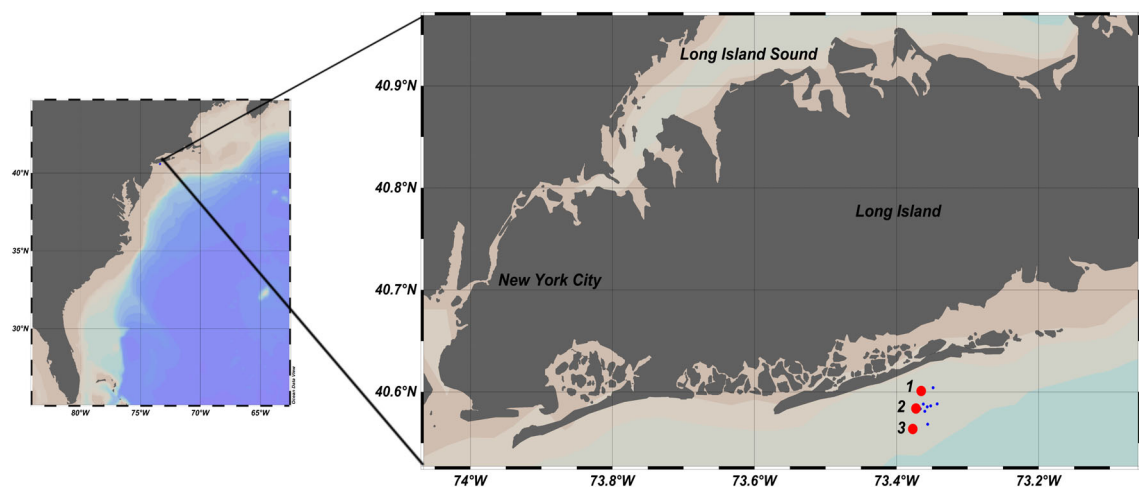


**Fig. 8.** Locations of 11 stations at the east part of the New York Bight, occupied during the Southwest Sewer district (SWSD) outfall discharge water quality study. Sta. 1, 2, and 3 were the source of the samples analyzed for the present study.

the Sta. 2 sample, the dominant polymer ( $n = 13$ ) was PTFE and the average size of these particles was  $3.4 \mu\text{m}$ . These 13 particles represented 12% of all counted particles, but their mass accounted for the 31% of the plastic mass at the three stations. The higher density of PTFE ( $\sim 2.2 \text{ g cm}^{-3}$ ) compared to PE, PS, and even CuPc ( $\sim 1.6 \text{ g cm}^{-3}$ ) also explains its contribution to total MP mass found at Sta. 2.

## Discussion

Our protocol enables precise identification of the polymers in MPs, accurate quantification of MPs down to  $0.46 \mu\text{m}$

diameter, and estimation of the volume of MPs, importantly enabling calculation of mass. While Raman microspectroscopy offers a powerful tool for the determination of MP volume, one of the drawbacks is that it is time-consuming relative to other methods (Anger et al. 2018). Here, we have demonstrated that the 3D Raman mapping approach can be used interchangeably with a 2D image analysis approach paired with a volume calculation for total plastic volume determination, which saves significantly on time and effort during analysis.

We also showed, with a limited sample set, it is possible that MPs  $< 5 \mu\text{m}$  can represent a majority of the plastic

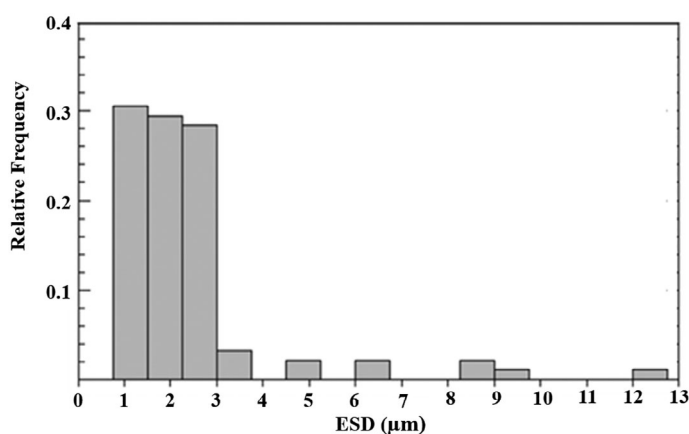


**Fig. 9.** Particle size frequency distribution of all MPs found in 0.5 L samples from three stations in Long Island coastal waters ( $N = 96$  MP particles). ESD of each particle was calculated using WiRE™ 5.1 image analyses software. Width of each bin was calculated using the Freedman-Diaconis rule (Wilks 2006).

inventory in discrete seawater samples. Furthermore, MP particle numbers are not robust proxies for accurately determining plastic loadings to natural waters. The methods outlined here facilitate detection of very small MP particles from environmental samples and thus help to further refine plastic budgets, including plastic polymer types, for a wide array of environmental reservoirs.

### Illuminating an underappreciated fraction of plastic pollution

Numerous studies have shown that MP particles  $\sim 0.3$ – $5$  mm are significantly more abundant than larger plastic particles in surface water samples (e.g., Erni-Cassola et al. 2017; Lindeque et al. 2020). However, these studies are based on techniques commonly used to sample plastics particles  $> 300$   $\mu\text{m}$  (e.g., plankton net collections), ignoring a potentially important fraction of marine plastic debris ( $< 300$   $\mu\text{m}$ ). Moreover, most analytical techniques for detection and identification of MPs do not provide chemical information on the polymer's composition, leading to false identification of plastic-like particles (Loder and Gerts 2015). For example, using microscopy for the analysis of environmental samples could lead to inflated estimates of MP abundances due to documented identification errors of 20–70% (Song et al. 2015; Shim et al. 2017). Consequently, particles  $< 300$   $\mu\text{m}$  in diameter have been mostly overlooked because of methodological limitations (Käppler et al. 2015; Anger et al. 2018). Nevertheless, as demonstrated by our field study this size fraction can be numerically dominant in some samples and can potentially represent a larger environmental threat than macroplastics (Ossmann et al. 2018).

Among several techniques that have been applied to the study of particles  $< 300$   $\mu\text{m}$ , Raman and FTIR microspectroscopies

enable accurate identification of plastic polymers using characteristic spectral features (Käppler et al. 2015; Primpke et al. 2020). FTIR is a complementary form of vibrational spectroscopy that also provides “molecular fingerprints” to accurately identify MP particles in the size range of  $\sim 10$ – $500$   $\mu\text{m}$  (Käppler et al. 2015). Improvements in this technique have been applied to analyze MP captured on filter membranes from environmental samples, which has reduced analytical time without sacrificing information needed to compute MP concentrations (Zarfl 2019; Primpke et al. 2020). Lorenz et al. (2019) were able to detect MP particles down to  $11$   $\mu\text{m}$  in sediment and surface water from the North Sea. Simon et al. (2018) identified several polymers in particles as small as  $26$   $\mu\text{m}$  in wastewater plant effluents. However, FTIR is known to under sample small MP particles ( $< 20$   $\mu\text{m}$ ) compared to Raman imaging, largely due to differences in spatial resolution dictated by the wavelengths of radiation used in these spectroscopies (Käppler et al. 2016; Cabernard et al. 2018; Zarfl 2019).

Raman microspectroscopy has been used increasingly to detect small MPs in environmental samples. For example,  $1$ – $10$   $\mu\text{m}$  MP particles were identified in seawater samples from various locations (Enders et al. 2015; Cabernard et al. 2018),  $> 5$   $\mu\text{m}$  MPs in a limnetic ecosystem (Imhof et al. 2018),  $5$ – $10$   $\mu\text{m}$  MPs from sediments (Käppler et al. 2016), and  $10$   $\mu\text{m}$  MPs in wastewater plants (Wolff et al. 2019). In addition, Schymanski et al. (2018) and Ossmann et al. (2018) detected small ( $1$ – $50$   $\mu\text{m}$ ) MP fragments in bottled drinking water. Using Raman microspectroscopy, we were able to accurately quantify particles from a coastal seawater sample down to diameters of  $\sim 1 \pm 0.46$   $\mu\text{m}$ .

In addition to being able to detect the presence of MPs  $< 20$   $\mu\text{m}$  to compute accurate inventories, it is also important to determine their volume and mass as concentrations alone are insufficient (Simon et al. 2018). In our limited field application, MP particle abundance at Sta. 2 was lower than at Sta. 1, but total MP mass was higher owing to slightly different particle sizes. Using FTIR and a similar approach to quantify MP mass in wastewater, Simon et al. (2018) found that relatively rare and large (mm scale) PP particles contributed the most to the total MP mass. This illustrates why accurate MP quantification and identification must be paired with accurate volume and mass determinations to accurately assess MP inventories. Using methods such as these to revise estimates of plastic loadings to natural waters is a step toward reconciling the mismatch between observed environmental inventories and plastic production and disposal rates.

The size range of most MP particles from our limited field campaign were between  $1$  and  $12.3$   $\mu\text{m}$  ESD, with 96% of the particles being less than  $5$   $\mu\text{m}$  and no MPs larger than  $200$   $\mu\text{m}$  captured in  $0.5$  L samples. MP concentrations found in the present study were much higher than previously reported for the North Atlantic (Lusher et al. 2014; Enders et al. 2015; Kanhai et al. 2017). While part of the difference could be due to sampling near the coast, these other studies only included particles  $> 7$   $\mu\text{m}$  (Enders et al.:  $7$ – $410$   $\mu\text{m}$ ; Kanhai et al.:  $0.25$ –

5 mm; Lusher et al.: 0.2–42 mm). However, Cabernard et al. (2018) reported MP concentrations in surface waters of the North Sea  $0.743 \text{ part L}^{-1}$ . These MP particles ranged between 1 and  $10 \mu\text{m}$  in diameter with 67% falling below  $5 \mu\text{m}$ , illustrating the numerical importance of the smallest size fraction to the total MP inventory.

In natural waters, MPs are suspended among much more numerous biogenic and mineral particles that can present challenges to their unambiguous detection. To illustrate, concentrations of particulate organic matter (POM) at the New York Bight vary from  $\sim 1 \text{ mg L}^{-1}$  on the longshore current/inner shelf zone to  $\sim 0.15 \text{ mg L}^{-1}$  at all depths over the continental shelf (Drake 1977). Based on our total MP inventories estimated from each polymer concentrations, volumes, and specific weights, we determined that  $\sim 1\text{--}3\%$  of the POM alone could be composed of MP particles in these surface water. Thus, our sample preparation and detection protocols appear adept at detecting and quantifying these anthropogenic particles that are rare compared to biogenic and lithogenic particles. From another perspective, MP contamination may have far-reaching impacts on current assessments of carbon speciation, cycling, and transport as well as its effects on marine biota.

### Potential for MP source tracking

Our method also offers the capability of MP source tracking based on polymer composition. We demonstrated that intensive 3D mapping enabled detection of multipolymer particles and permitted mapping each polymer's distribution within a single particle, as well as individual mass estimations for each polymer component. To our knowledge, no other method is able to provide mass contributions of multiple polymers in individual MP particles at the same resolution as Raman. We were also able to infer that a particular multipolymer particle was a product of the plastic recycling industry due to its unique composition.

Another important capability of Raman microspectroscopy in MP analysis is its ability to detect pigments and additives used during plastics manufacturing. One of the most common spectra found in environmental samples was that of phthalocyanine copper blue (CuPc). CuPc is a very important organic pigment used in manufacturing plastics and is used widely to color PP and PE, since these resins cannot be colored by inorganic dyes (Lewis 2003; Weadon and Martin 2003). CuPc has been detected previously by Raman microspectroscopy in marine water and sediment samples (Claessens et al. 2011; Zhao et al. 2017). This pigment was detected at all three of our field stations as a pure component, comprising entire particles (3D volume measurements), as well as mixtures with other polymers (PE, PP, and PTFE). Another important additive found in our field samples was titanium dioxide ( $\text{TiO}_2$ ), which has been used widely in plastics manufacturing as an additive to minimize brittleness, fading, and cracking that plastics and other materials are prone to over prolonged light exposures (Gázquez et al. 2014).

### Comments and recommendations

We have demonstrated that this methodology is suitable for quantification of MP particles as small as  $0.46 \mu\text{m}$  from water samples and collected on filters, and enables calculation of specific MP abundance, chemical composition, size, and mass. However, there are three aspects of our methodology requiring further development in order to reduce total time for sample and data analysis. First, Raman microspectroscopy analysis can be time-consuming especially when the goal is accurate analysis of particles smaller than  $10 \mu\text{m}$  in complex environmental samples. We were able to establish a 90 min analysis time per ROI, with each ROI defined as a  $100 \times 100 \mu\text{m}$  grid in the camera image, 0.7 s spectrum acquisition times and using  $1 \times 1 \mu\text{m}$  step size on the automated stage. This allowed us to map 33 ROI per sample in approximately 50 h, yielding adequate spatial coverage of the filter surface to minimize analytical uncertainty. We consider the trade-off between measurement time and representativeness of our methodology to be acceptable, but not optimal.

We recognize the need to reduce the total time for Raman analysis. At the outset, we opted for the fixed grid mapping of 10,000 points within an individual ROI rather than searching for individual particles. This was necessary because small and colorless MPs are nearly impossible to recognize visually when captured on  $\text{Al}_2\text{O}_3$  filters due to poor contrast. Brandt et al. (2020) suggested that acquiring an optical image of the entire filter and then running an automated particle recognition algorithm that identifies all present particles is a viable alternative to the point-by-point mapping approach. This approach reduces the number of spectra collected and requisite data analysis, thereby accelerating data throughput. However, particles  $< 5 \mu\text{m}$  can be overlooked if particles are not sufficiently contrasted from the filter and if a suitable image segmentation algorithm is not applied to identified particles.

One possible option to rapidly recognize and interrogate smaller particles may be to combine an MP staining technique with Raman microspectroscopy. Nile red dye (9-diethylamino-5H-benzo[a]phenoxazine-5-one) is a likely candidate that has been demonstrated to stain many types of lipophilic particles, including MPs (Erni-Cassola et al. 2017; Tammenga 2017). Nile red is unlikely to interfere with Raman interrogation using a 633 nm laser because its excitation maximum is at 552 nm and it does not absorb light above 600 nm, so it is promising for this application. Using the epifluorescence capabilities of the Raman microspectroscope, coordinates of high-contrast fluorescent particles can be instantly recorded in an optical field. Then the instrument's particle recognition software (e.g., Renishaw WiRE™ 5.2) can direct the automated stage to acquire single 0.5–1.0 s spectra from each recorded x-y coordinate. Coupling these techniques could significantly reduce the number of spectra needed to survey an optical field, enable more extensive sampling of an individual filter, reduce overall sampling time, and

reduce cost per sample. Klein and Fischer (2019) demonstrated that Nile red dissolved in chloroform was a good alternative dyeing agent to recognize airborne MP particles. We note that they manually transferred a subset of filter-collected  $> 50 \mu\text{m}$  particles to a slide before determining polymer composition by Raman microspectroscopy. We are now exploring Nile Red, other stains, and alternative imaging approaches to efficiently recognize MPs in aquatic samples and accelerate quantitative analysis.

Second, processing Raman spectra can also be time-consuming and laborious. In order to accelerate of data processing, we used a semiautomated approach (non-negative least squares correlation method) to create chemical maps across multiple ROIs. Nonetheless, some manual review and data curation was still necessary. Consequently, development of automatable and faster tools to ensure the correct analysis of large datasets is imperative. Such tools already exist for FTIR (Systematic Identification of Microplastic in the Environment [https://simple-plastics.eu/]). The Raman version of this software is in its beta stage. However, another promising option for the automation of spectral data analysis is the Spectral Library of Plastic Particles (SLoPP) and Spectral Library of Plastic Particles aged in the Environment (SLoPP-E) for Raman spectroscopy (Munno et al. 2020). Unfortunately, these libraries are not stand-alone and were designed to be integrated into KnowItAll Raman Spectral Library (BIO-RAD®) which is a commercial, subscription-based spectral reference library and expert search software. This translates into an extra financial burden for already limited MP research budgets. Open access tools will increase accessibility to Raman spectral analysis, enable more extensive sampling of filters to assure accurate results, increase data throughput, decrease analytical costs, and enhance data quality and consistency.

Finally, our algorithm for calculating MP particle mass in environmental samples assumes an idealized particle geometry for “2D volume” calculations and a mean specific weight for a given polymer for mass estimations. We know that a portion of the MP pool will not conform strictly to ellipsoid geometry. Furthermore, actual specific weights of environmental MP polymers may depart from the mean depending on source and weathering. We also recognize that MP particle concentrations extrapolated from filter-based counts introduces uncertainty that can be difficult to constrain. We attempted to reduce sources of uncertainty by first selecting a geometric model that approximated many possible shapes and could be applied broadly while also minimizing required microscopic measurements. Second, for each identified polymer, we considered the mean and standard error from a robust range of published density values (see Supporting Information Table S4). Lastly, as discussed by Loder et al. (2015), uneven MP particle distributions on filters lead to a significant bias when total particle concentrations are extrapolated from subsampling a filter. Introducing a backing filter to distribute

vacuum pressure more uniformly appeared to reduce particle distribution heterogeneity, but it was still relatively high in field samples. In theory, filtering larger water volumes to capture more particles per  $\text{mm}^2$  of filter surface could significantly reduce counting error. In practice however, larger filtration volumes also will introduce more non-MP particles that can obscure MPs and clog pores. Among the reported uncertainties for volumes, densities, particle numbers, and masses, the relative error for particle number was the highest. We continue to explore strategies to reduce analytical uncertainties, especially focusing on balancing counting error with analysis time while minimizing artifacts.

## References

- Alimi, O. S., L. M. Hernandez, and N. Tufenkji. 2018. Microplastics and nanoplastics in aquatic environments: Aggregation, deposition, and enhanced contaminant transport. *Environ. Sci. Technol.* **52**: 1704–1724. doi:10.1021/acs.est.7b05559
- Anger, P. M., E. von der Esch, T. Baumann, M. Elsner, R. Niessner, and N. P. Ivleva. 2018. Raman microspectroscopy as a tool for microplastic particle analysis. *Trends Analyt. Chem.* **109**: 214–226. doi:10.1016/j.trac.2018.10.010
- Araujo, C. F., M. M. Nolasco, A. M. P. Ribeiro, and P. J. A. Ribeiro-Claro. 2018. Identification of microplastics using Raman spectroscopy: Latest developments and future prospects. *Water Res.* **142**: 426–440. doi:10.1016/j.watres.2018.05.060
- Arthur, C., J. Baker, and H. Bamford (eds). 2009. Proceedings of the International Research Workshop on the Occurrence, Effects, and Fate of Microplastic Marine Debris, NOAA Technical Memorandum NOS-OR&R-30, p. 530.
- Brandt, J., and others. 2020. High-throughput analyses of microplastic samples using Fourier transform infrared and Raman spectrometry. *Appl. Spectrosc.* **74**: 1185–1197. doi:10.1177/0003702820932926
- Cabernard, L., L. Roscher, C. Lorenz, G. Gerdt, and S. Primpke. 2018. Comparison of Raman and Fourier transform infrared spectroscopy for the quantification of microplastics in the aquatic environment. *Environ. Sci. Technol.* **52**: 13279–13288. doi:10.1021/acs.est.8b03438
- Claessens, M., S. De Meester, L. Van Landuyt, K. De Clerck, and C. R. Janssen. 2011. Occurrence and distribution of microplastics in marine sediments along the Belgian coast. *Mar. Pollut. Bull.* **62**: 2199–2204. doi:10.1016/j.marpolbul.2011.06.030
- Conkle, J. L., C. D. Báez Del Valle, and J. W. Turner. 2018. Are we underestimating microplastic contamination in aquatic environments? *Environ. Manag.* **61**: 1–8. doi:10.1007/s00267-017-0947-8
- Covernton, G. A., C. M. Pearce, H. J. Gurney-Smith, S. G. Chastain, P. S. Ross, J. F. Dower, and S. Dudas. 2019. Size and shape matter: A preliminary analysis of microplastic

- sampling technique in seawater studies with implications for ecological risk assessment. *Sci. Total Environ.* **667**: 124–132. doi:[10.1016/j.scitotenv.2019.02.346](https://doi.org/10.1016/j.scitotenv.2019.02.346)
- Drake, D. 1977. Suspended particulate matter in the New York Bight Apex, Fall 1973. *SEPM J. Sediment. Res.* **47**: 209–228. doi:[10.1306/212f7130-2b24-11d7-8648000102c1865d](https://doi.org/10.1306/212f7130-2b24-11d7-8648000102c1865d)
- Eagan, J. M., J. Xu, R. Di Girolamo, C. M. Thurber, C. W. Macosko, A. M. La Pointe, F. Bates, and G. Coates. 2017. Combining polyethylene and polypropylene: Enhanced performance with PE/iPP multiblock polymers. *Science* **355**: 814–816. doi:[10.1126/science.aah5744](https://doi.org/10.1126/science.aah5744)
- Enders, K., R. Lenz, C. A. Stedmon, and T. G. Nielsen. 2015. Abundance, size and polymer composition of marine microplastics  $\geq 10 \mu\text{m}$  in the Atlantic Ocean and their modelled vertical distribution. *Mar. Pollut. Bull.* **100**: 70–81. doi:[10.1016/j.marpolbul.2015.09.027](https://doi.org/10.1016/j.marpolbul.2015.09.027)
- Engel, A. 2009. Determination of marine gel particles, p. 125–142. *In* O. Wurl [ed.], *In Practical guidelines for the analysis of seawater*. CRC Press.
- Eriksen, M., L. C. M. Lebreton, H. S. Carson, M. Thiel, C. J. Moore, J. C. Borerro, F. Galgani, and P. Ryan. 2014. Plastic pollution in the world's oceans: More than 5 trillion plastic pieces weighing over 250,000 tons afloat at sea. *PLoS One* **9**: e111913. doi:[10.1371/journal.pone.0111913](https://doi.org/10.1371/journal.pone.0111913)
- Erni-Cassola, G., M. I. Gibson, R. C. Thompson, and J. A. Christie-Oleza. 2017. Lost, but found with Nile red: A novel method for detecting and quantifying small microplastics (1mm to  $20 \mu\text{m}$ ) in environmental samples. *Environ. Sci. Technol.* **51**:13641–13648. doi:[10.1021/acs.est.7b04512](https://doi.org/10.1021/acs.est.7b04512)
- Frère, L., I. Paul-Pont, J. Moreau, P. Soudant, C. Lambert, A. Huvet, and E. Rinnert. 2016. A semi-automated Raman micro-spectroscopy method for morphological and chemical characterizations of microplastic litter. *Mar. Pollut. Bull.* **113**: 461–468. doi:[10.1016/j.marpolbul.2016.10.051](https://doi.org/10.1016/j.marpolbul.2016.10.051)
- Gázquez, M. J., J. P. Bolívar, R. Garcia-Tenorio, and F. Vaca. 2014. A review of the production cycle of titanium dioxide pigment. *Mater. Sci. Appl.* **5**: 441–458. doi:[10.4236/msa.2014.57048](https://doi.org/10.4236/msa.2014.57048)
- Harris, D. 2010. Quantitative chemical analysis, 8th ed. p. 928. W.H. Freeman and Company, New York. ISBN: 978-1-4641-3538-5
- Hidalgo-Ruz, V., L. Gutow, R. C. Thompson, and M. Thiel. 2012. Microplastics in the marine environment: A review of the methods used for identification and quantification. *Environ. Sci. Technol.* **46**: 3060–3075. doi:[10.1021/es2031505](https://doi.org/10.1021/es2031505)
- Hillebrand, H., C. D. Dürselen, D. Kirschtel, U. Pollinger, and T. Zohary. 1999. Biovolume calculation for pelagic and benthic microalgae. *J. Phycol.* **35**: 403–424. doi:[10.1046/j.1529-8817.1999.3520403.x](https://doi.org/10.1046/j.1529-8817.1999.3520403.x)
- Hubo, S., L. Delva, N. Van Damme, and K. Ragaert. 2016. Blending of recycled mixed polyolefins with recycled polypropylene: Effect on physical and mechanical properties. *AIP Conf. Proc.* **1779**: 140006-1–140006-5. doi:[10.1063/1.4965586](https://doi.org/10.1063/1.4965586)
- Imhof, H. K., J. Schmid, R. Niessner, N. P. Ivleva, and C. Laforsch. 2012. A novel, highly efficient method for the separation and quantification of plastic particles in sediments of aquatic environments. *Limnol. Oceanogr.: Methods* **10**: 524–537. doi:[10.4319/lom.2012.10.524](https://doi.org/10.4319/lom.2012.10.524)
- Imhof, H. K., A. C. Wiesheu, P. M. Anger, R. Niessner, N. P. Ivleva, and C. Laforsch. 2018. Variation in plastic abundance at different lake beach zones - a case study. *Sci. Total Environ.* **613–614**: 530–537. doi:[10.1016/j.scitotenv.2017.08.300](https://doi.org/10.1016/j.scitotenv.2017.08.300)
- Jambeck, J., R. Geyer, C. Wilcox, T. R. Siegler, M. Perryman, A. Andrady, R. Narayan, and K. Law. 2015. Plastic waste inputs from land into the ocean. *Science* **347**: 3–6. doi:[10.1126/science.1260352](https://doi.org/10.1126/science.1260352)
- Kanhai, L. D. K., R. Officer, O. Lyashevskaya, R. C. Thompson, and I. O'Connor. 2017. Microplastic abundance, distribution and composition along a latitudinal gradient in the Atlantic Ocean. *Mar. Pollut. Bull.* **115**: 307–314. doi:[10.1016/j.marpolbul.2016.12.025](https://doi.org/10.1016/j.marpolbul.2016.12.025)
- Käppler, A., F. Windrich, M. G. J. Löder, M. Malanin, D. Fischer, M. Labrenz, K. Eichhorn, and B. Voit. 2015. Identification of microplastics by FTIR and Raman microscopy: A novel silicon filter substrate opens the important spectral range below  $1300 \text{ cm}^{-1}$  for FTIR transmission measurements. *Anal. Bioanal. Chem.* **407**: 6791–6801. doi:[10.1007/s00216-015-8850-8](https://doi.org/10.1007/s00216-015-8850-8)
- Käppler, A., D. Fischer, S. Oberbeckmann, G. Schernewski, M. Labrenz, K. Eichhorn, and B. Voit. 2016. Analysis of environmental microplastics by vibrational microspectroscopy: FTIR, Raman or both? *Anal. Bioanal. Chem.* **408**: 8377–8391. doi:[10.1007/s00216-016-9956-3](https://doi.org/10.1007/s00216-016-9956-3)
- Klein, M., and E. K. Fischer. 2019. Microplastic abundance in atmospheric deposition within the metropolitan area of Hamburg, Germany. *Sci. Total Environ.* **685**: 96–103. doi:[10.1016/j.scitotenv.2019.05.405](https://doi.org/10.1016/j.scitotenv.2019.05.405)
- Lewis, P. A. 2003. Organic colorants, p. 100–126. *In* R. A. Charvat [ed.], *Coloring of plastics*. Hoboken, NJ: Wiley Intersciences, John Wiley & Sons, Inc.
- Lindeque, P. K., and others. 2020. Are we underestimating microplastic abundance in the marine environment? A comparison of microplastic capture with nets of different mesh-size. *Environ. Pollut.* **265**: 114721. doi:[10.1016/j.envpol.2020.114721](https://doi.org/10.1016/j.envpol.2020.114721)
- Löder, M. G. J., and G. Gerdt, 2015. Methodology Used for the Detection and Identification of Microplastics. p. 114721. *In* M. Bergmann, L. Gutow, M. Klages [eds.], *A Critical Appraisal. Marine Anthropogenic Litter*. Springer, Cham. doi:[10.1007/978-3-319-16510-3\\_8](https://doi.org/10.1007/978-3-319-16510-3_8)
- Loder, M., M. Kuczera, S. Mintenig, C. Lorenz, and G. Gerdt, 2015. Focal plane array detector-based micro-Fourier-transform infrared imaging for the analysis of microplastics in environmental samples. *Environ. Chem.* **12**: 563–581. doi:[10.1071/EN14205](https://doi.org/10.1071/EN14205)

- Lohmann, R. 2017. Microplastics are not important for the cycling and bioaccumulation of organic pollutants in the oceans—but should microplastics be considered POPs themselves? *Integr. Environ. Assess. Manag.* **13**: 460–465. doi:10.1002/ieam.1914
- Lorenz, C., L. Roscher, M. S. Meyer, L. Hildebrandt, J. Prume, M. G. J. Löder, S. Primpke, and G. Gerdt. 2019. Spatial distribution of microplastics in sediments and surface waters of the southern North Sea. *Environ. Pollut.* **252**: 1719–1729. doi:10.1016/j.envpol.2019.06.093
- Lusher, A. L., A. Burke, I. O'Connor, and R. Officer. 2014. Microplastic pollution in the Northeast Atlantic Ocean: Validated and opportunistic sampling. *Mar. Pollut. Bull.* **88**: 325–333. doi:10.1016/j.marpolbul.2014.08.023
- Martin, J., A. Lusher, R. C. Thompson, and A. Morley. 2017. The deposition and accumulation of microplastics in marine sediments and bottom water from the Irish continental shelf. *Sci. Rep.* **7**: 1–9. doi:10.1038/s41598-017-11079-2
- Mintening, S., I. Int-Veen, M. Loder, S. Primpke, and G. Gerdt. 2017. Identification of microplastic in effluents of waste water treatment plants using focal plane array-based micro-Fourier-transform infrared imaging. *Water Res.* **108**: 365–372. doi:10.1016/j.watres.2016.11.015
- Munno, K., H. De Frond, B. O'Donnell, and C. M. Rochman. 2020. Increasing the accessibility for characterizing microplastics: Introducing new application-based and spectral libraries of plastic particles (SLoPP and SLoPP-E). *Anal. Chem.* **92**: 2443–2451. doi:10.1021/acs.analchem.9b03626
- Oberbeckmann, S., B. Kreikemeyer, M. Labrenz, and J. P. Harrison. 2018. Environmental factors support the formation of specific bacterial assemblages on microplastics. *Front. Microbiol.* **8**: 2709. doi:10.3389/fmicb.2017.02709
- Ossmann, B. E., G. Sarau, H. Holtmannspötter, M. Pischetsrieder, S. H. Christiansen, and W. Dicke. 2018. Small-sized microplastics and pigmented particles in bottled mineral water. *Water Res.* **141**: 307–316. doi:10.1016/j.watres.2018.05.027
- Primpke, S., C. Lorenz, and G. Gerdt. 2017. Analytical methods an automated approach for microplastics analysis using focal plane array (FPA) FTIR microscopy and image analysis. *Anal. Methods* **9**: 1499–1511. doi:10.1039/C6AY02476A
- Primpke, S., and others. 2020. Critical assessment of analytical methods for the harmonized and cost-efficient analysis of microplastics. *Appl. Spectrosc.* **74**: 1012–1047. doi:10.1177/0003702820921465
- Rios, L., J. Patrick, C. Moore, and U. Narayan. 2010. Quantitation of persistent organic pollutants adsorbed on plastic debris from the Northern Pacific Gyre's "eastern garbage patch". *J. Environ. Monit.* **12**: 2226–2236. doi:10.1039/c0em00239a
- Schymanski, D., C. Goldbeck, H. U. Humpf, and P. Fürst. 2018. Analysis of microplastics in water by micro-Raman spectroscopy: Release of plastic particles from different packaging into mineral water. *Water Res.* **129**: 154–162. doi:10.1016/j.watres.2017.11.011
- Shim, W. J., S. H. Hong, and S. E. Eo. 2017. Identification methods in microplastic analysis: A review. *Anal. Methods* **9**: 1384–1391. doi:10.1039/C6AY02558G
- Simon, M., N. van Alst, and J. Vollertsen. 2018. Quantification of microplastic mass and removal rates at wastewater treatment plants applying focal plane array (FPA)-based Fourier transform infrared (FT-IR) imaging. *Water Res.* **142**: 1–9. doi:10.1016/j.watres.2018.05.019
- Song, Y. K., S. H. Hong, M. Jang, G. M. Han, M. Rani, J. Lee, and W. Shim. 2015. A comparison of microscopic and spectroscopic identification methods for analysis of microplastics in environmental samples. *Mar. Pollut. Bull.* **93**: 202–209. doi:10.1016/j.marpolbul.2015.01.015
- Tagg, A. S., M. Sapp, J. P. Harrison, and J. J. Ojeda. 2015. Identification and quantification of microplastics in wastewater using focal plane array-based reflectance micro-ft-ir imaging. *Anal. Chem.* **87**: 6032–6040. doi:10.1021/acs.analchem.5b00495.
- Tammaing, M. 2017. Nile red staining as a subsidiary method for microplastic quantification: A comparison of three solvents and factors influencing application reliability. *SDRP J. Earth Sci. Environ. Stud.* **2**: 165–172. doi:10.15436/jeses.2.2.1
- Weadon, C., and W. Martin. 2003. Soluble dyes. p. 175–184. *In* R. A. Charvat [ed.], *Coloring of plastics*. Hoboken, NJ: Wiley Intersciences, John Wiley & Sons, Inc.
- Wilks, D. 2006. Statistical methods in the atmospheric sciences, 2nd ed. *In* R. Dmowska, D. Hartmann, and T. Rossy [eds.], *New York, NY: Elsevier*. doi:10.1007/978-0-387-87811-9\_6.
- Wolff, S., J. Kerpen, J. Prediger, L. Barkmann, and L. Müller. 2019. Determination of the microplastics emission in the effluent of a municipal waste water treatment plant using Raman microspectroscopy. *Water Res. X* **2**: 100014. doi:10.1016/j.wroa.2018.100014
- Woodall, L. C., and others. 2014. The deep sea is a major sink for microplastic debris subject. *J. Soc. Open Sci.* **1**: 1–8.
- Zada, L., H. A. Leslie, A. D. Vethaak, G. H. Tinnevelt, J. J. Jansen, J. F. de Boer, and F. Ariese. 2018. Fast microplastics identification with stimulated Raman scattering microscopy. *J. Raman Spectrosc.* **49**: 1136–1144. doi:10.1002/jrs.5367
- Zarfl, C. 2019. Promising techniques and open challenges for microplastic identification and quantification in environmental matrices. *Anal. Bioanal. Chem.* **411**: 3743–3756. doi:10.1007/s00216-019-01763-9
- Zettler, E. R., T. J. Mincer, and L. A. Amaral-Zettler. 2013. Life in the "plastisphere": Microbial communities on plastic marine debris. *Environ. Sci. Technol.* **47**: 7137–7146. doi:10.1021/es401288x

Zhang, H. 2017. Transport of microplastics in coastal seas. *Estuar. Coast. Shelf Sci.* **199**: 74–86. doi:[10.1016/j.ecss.2017.09.032](https://doi.org/10.1016/j.ecss.2017.09.032)

Zhao, S., M. Danley, J. E. Ward, D. Li, and T. J. Mincer. 2017. An approach for extraction, characterization and quantitation of microplastic in natural marine snow using Raman microscopy. *Anal. Methods* **9**: 1470–1478. doi:[10.1039/c6ay02302a](https://doi.org/10.1039/c6ay02302a)

### Acknowledgments

The authors are grateful to Elizabeth Suter for thoughtful review of manuscript drafts and to Larissa Chraim and Craig Young for laboratory and data analysis assistance. Also, Karin Schweitzer for collecting environmental samples. Research was partially supported by a Stony Brook University (SBU) seed grant. All Raman spectral data were produced in SBU's School of Marine and Atmospheric Sciences' NAno Raman Molecular

Imaging Laboratory (NARMIL), a community resource dedicated to environmental science applications and founded with NSF-MRI grant OCE-1336724.

### Conflict of Interest

None declared.

*Submitted 22 September 2020*

*Revised 10 February 2021*

*Accepted 29 March 2021*

*Associate editor: Robert Chen*